Received: 31 March 2022 | Revised: 21 June 2022 | Accepted: 14 July 2022

DOI: 10.1002/suco.202200311

ARTICLE

fib CEB-FIP WILEY

A new cyclic model for FRP-confined rubberized concrete

Samar Raffoul[1] | **David Escolano Margarit**[2] | **Reyes Garcia**[3] | **Maurizio Guadagnini**[4] | **Kypros Pilakoutas**[4]

[1]School of Civil Engineering, University College Dublin, Dublin, Ireland

[2]Department of Mechanical Engineering, Polytechnic University of Madrid, Madrid, Spain

[3]School of Engineering, The University of Warwick, Coventry, UK

[4]Department of Civil and Structural Engineering, The University of Sheffield, Sheffield, UK

Correspondence
Samar Raffoul, School of Civil Engineering, University College Dublin, Dublin, Ireland.
Email: samar.raffoul@ucd.ie

Funding information
H2020 Marie Skłodowska-Curie Actions, Grant/Award Numbers: 101029972, 658248; European Union Seventh Framework Programme, Grant/Award Number: 603722

Abstract

This article proposes a new constitutive model for the cyclic behavior of rubberized concrete confined with fiber-reinforced polymer (FRP) sheets. The model is calibrated with experimental results from 18 confined rubberized concrete (CRuC) cylinders tested in cyclic compression. The cylinders had 60% total aggregate volume replacement with recycled tyre rubber. Parameters investigated include the type of confining material (Carbon or Aramid FRP) and number of layers (two, three, or four). The results indicate that using FRP confinement leads to a strong (up to 100 MPa) and highly deformable (axial strains up to 7%) rubberized concrete that can be used in structural applications. The proposed constitutive model predicts accurately the material response under cyclic loading and can thus be used for design/analysis of highly deformable components made of FRP CRuC. This article contributes toward the development of advanced constitutive models for FRP CRuC, thus promoting the wider use of recycled materials in construction industry.

KEYWORDS

composite materials, cyclic model, FRP confinement, highly deformable concrete, rubberized concrete

1 | INTRODUCTION

In recent years, numerous studies have examined the use of end-of-life tyre rubber as mineral aggregate replacement to produce rubberized concrete (RuC) composites. The addition of rubber in concrete enables the construction of highly deformable structural components,[1–3] particularly when large volumes of rubber are used.[4,5] Nevertheless, the inclusion of high volumes of recycled rubber in concrete reduces the workability of the fresh mix[6–8] and reduces the compressive strength and stiffness of RuC[7,9] when compared to conventional concrete. Recent research by Raffoul et al.[10] has shown that the fresh properties of RuC can be improved by optimizing the concrete mix parameters, leading to RuC with high rubber content (60% of the total aggregate volume) and good workability, homogeneity, and cohesiveness. However, a significant reduction (up to 90%) in strength is typically observed at such high rubber contents,[10] thus hindering the use of RuC in structural applications where medium to high-strength concrete is used.

Recent studies have shown that externally bonded fiber-reinforced polymer (FRP) or steel confinement can

Discussion on this paper must be submitted within two months of the print publication. The discussion will then be published in print, along with the authors' closure, if any, approximately nine months after the print publication.

be used to produce high-strength confined rubberized concrete (CRuC).[11–15] For example, Youssf et al.[12] reported compressive strengths of 112.5 MPa in RuC cylinders (20% rubber replacing the sand volume) cast in preformed carbon FRP (CFRP) tubes. While the above use of confinement somehow improved the strength of RuC, it had marginal influence on the concrete deformability. Indeed, the maximum axial strains (1.8%) reported by Youssf et al.[12] were comparable to, or even lower, than those achieved in conventional FRP-confined concrete.[16] Duarte et al.[14] reported a 50% increase in ductility by confining RuC columns with cold-formed steel tubes, albeit observing a lower confinement effectiveness due to the lower dilation angle of RuC. Although promising in terms of strength enhancement, the limited increase in deformation capacity observed in previous studies can be attributed to the use of relatively low rubber contents (20% rubber replacing sand volume[12] or 15% rubber replacing total aggregate volume[14]), which in turn prevents the full exploitation of the large lateral expansion capacity of rubber aggregates. To address these shortcomings, Raffoul et al.[17] used Aramid FRP (AFRP) jackets to confine high rubber content RuC cylinders (60% total aggregate volume replacement) to significantly increase both their strength and deformation capacity. Such highly deformable FRP CRuC with compressive strengths greater than 70 MPa and axial strains of around 5% can be used in numerous structural applications where large deformability is required, like in plastic hinges of buildings/bridges or base isolators. Raffoul et al.[18] also identified that FRP CRuC cylinders with high rubber contents exhibit large initial lateral strains that lead to early activation of the passive confinement pressure, which in turn results in higher confinement effectiveness (with strength and strain enhancement ratios of 11 and 45, respectively). Indeed, stress path dependence of passively confined concrete and the effects of concrete dilation characteristics on confinement effectiveness have been documented in previous literature.[19,20] Raffoul et al.[18] proposed an active confinement constitutive model for FRP CRuC that employs an incremental iterative procedure based on lateral-to-axial strain compatibilities at given confinement ratios. While such model predicts accurately the monotonic behavior of AFRP/CFRP CRuC cylinders subject to axial load, practical design-oriented cyclic constitutive models for CRuC are still needed to simplify the design of highly deformable structures.

This study proposes a new design-oriented constitutive model to predict the cyclic behavior of FRP CRuC. To achieve this, the uniaxial compressive behavior of FRP CRuC is initially investigated by testing cylinders with high rubber contents (60% of the total aggregate volume) under cyclic load. The test results are examined in detail to determine the main factors influencing FRP CRuC behavior. The new cyclic model for FRP CRuC is then proposed based on the experimental evidence, and the main conclusions are briefly summarized. This article contributes toward the development of advanced constitutive models for highly deformable FRP-confined rubberized concrete so as to promote the wider use of recycled materials in the construction industry. This study was part of the FP7 EU-funded project Anagennisi, which aimed to develop high-value uses for all tyre components in concrete.[21]

2 | EXPERIMENTAL DATABASE

This study builds on the results of a previous experimental program by the authors[18] that examined the influence of FRP type (AFRP or CFRP) and confinement ratio (two, three, or four layers of FRP) on the uniaxial compressive behavior of CRuC. The study included 30 RuC cylinders (100 mm diameter × 200 mm height) confined with externally bonded FRP jackets and tested in monotonic (12 cylinders) and cyclic (18 cylinders) uniaxial compression (Figure 1). Both monotonic and cyclic loading data were used in this study to develop the envelope curve of the stress–strain behavior of FRP CRuC.

The RuC mix used in this study had a high rubber content that replaced 60% of the fine and coarse mineral aggregates by volume and was developed in a previous study following substantial research into the effects of

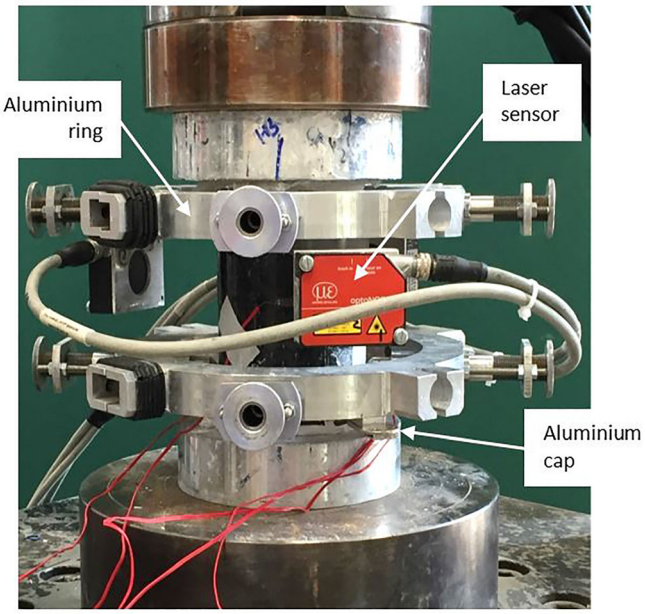

FIGURE 1 Typical test setup of CRuC cylinders subject to uniaxial compression

TABLE 1 Key test results from cyclic and monotonic tests on FRP CRuC cylinders

ID	K_{jn}	f_{cc} (MPa)	ε_{cc} (%)	ε_{ccl} (%)	f_{cr} (MPa)	ε_{cr} (%)	f_0 (MPa)	$E_{c,0}$ (GPa)
2LA-C	119.0	38.7 (1.5)	3.71 (0.4)	1.46 (0.0)	12.2 (0.6)	0.19 (0.02)	13.2 (0.2)	9.3 (1.4)
2LA-M		42.3 (3.4)	4.19 (0.6)	1.68 (0.4)	8.4 (0.4)	0.11 (0.01)	11.5 (0.0)	11.1 (0.5)
3LA-C	178.5	69.9 (0.3)	5.53 (0.5)	1.60 (0.3)	14.5 (3.8)	0.20 (0.06)	12.6 (0.7)	12.4 (2.5)
3LA-M		69.9 (5.2)	5.24 (0.4)	1.51 (0.2)	12.0 (1.1)	0.14 (0.03)	11.9 (0.4)	13.6 (1.5)
4LA-C	238.1	90.0 (0.2)	5.81 (0.5)	1.65 (0.1)	13.6 (2.3)	0.17 (0.01)	18.5 (2.7)	11.1 (3.1)
4LA-M		96.1 (7.5)	6.4 (1.0)	1.60 (0.3)	14.5 (1.2)	0.25 (0.02)	14.6 (1.6)	8.4 (0.6)
2LC-C	183.6	33.9 (2.2)	2.37 (0.4)	0.81 (0.1)	12.5 (1.1)	0.24 (0.08)	15.9 (1.4)	8.2 (1.8)
2LC-M		31.7 (2.7)	2.21 (0.7)	0.68 (0.1)	11.3 (0.1)	0.17 (0.01)	16.5 (0.1)	10.4 (0.8)
3LC-C	275.5	42.7 (12.3)	2.96 (0.9)	0.84 (0.3)	11.1 (2.5)	0.20 (0.06)	18.3 (2.2)	9.2 (0.7)
3LC-M		48.8 (3.4)	2.56 (0.9)	0.80 (0.1)	16.0 (−)	0.29 (−)	17.3 (−)	7.0 (1.1)
4LC-C	367.3	58.0 (8.1)	3.51 (0.7)	0.73 (0.3)	14.0 (2.4)	0.22 (0.02)	17.8 (0.6)	9.1 (1.0)
4LC-M		62.7 (1.5)	3.66 (0.6)	0.83 (0.0)	15.4 (0.0)	0.24 (0.02)	16.0 (1.0)	9.6 (2.3)

Note: Numbers in brackets indicate the standard deviation calculated from tests on three samples for the cyclically loaded cylinders and two samples for the monotonically loaded cylinders.

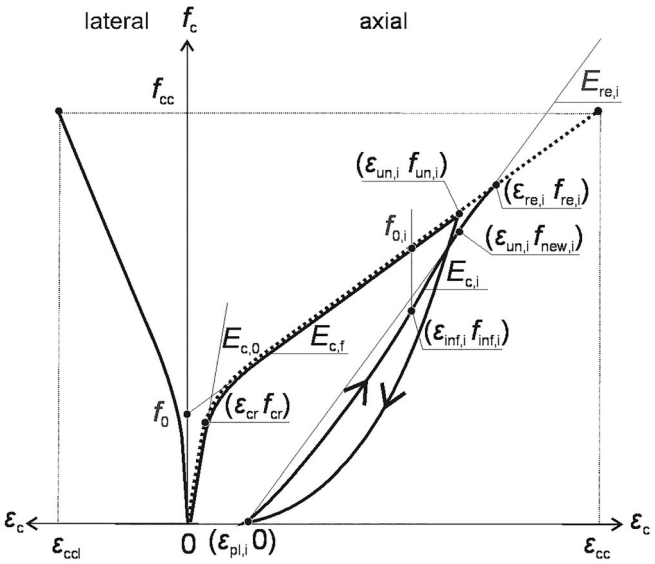

FIGURE 2 Key parameters of cyclic behavior of FRP CRuC

plasticizers, particle packing, and other mix parameters on the rheology and fresh and hardened mechanical properties of concrete with high rubber content.[10] The significance of achieving "ideal packing" in concrete using filler/binder materials and plasticizers and their influence on concrete properties has been well established in the literature.[10,22–26] The concrete mix proportions were (kg/m^3) (i) 340 of Portland Limestone cement with 10–15% limestone content (CEMII-52.5 N); (ii) 42.5 of silica fume; (iii) 42.5 of pulverized fuel ash; (iv) 149 L of water (water to binder ratio of 0.35); (v) 7.6 L of water reducing admixtures (2.5 L of plasticizer and 5.1 L of superplasticiser); (vi) 400.4 of round river washed gravel (coarse aggregates, sized 5–20 mm) and 328 of medium grade river washed sand (fine aggregates, sized 0–5 mm); and (vii) 181.3 of coarse rubber (sized 5–10 mm) and 148.5 of fine rubber (sized 0–5 mm). A characterization of the rubber particles used can be found in Reference 10. The optimized concrete mix presented adequate workability, good cohesion, and limited segregation.[10] Average slump and flow table values were 40 mm and 410 mm, respectively. The 28-day mechanical properties of three unconfined RuC cylinders subjected to uniaxial compression were mean compressive strength f_{co} = 7.6 MPa [standard deviation (SD) = 1.3 MPa], mean strain at peak stress $\varepsilon_{co} = 1350\mu\varepsilon$ (SD = $200\mu\varepsilon$), and mean modulus of elasticity $E_{c,0}$ = 10.3 GPa (SD = 1.8 GPa). Full details of the concrete mix development and concrete production procedure can be found in Raffoul et al.[10]

TABLE 2 FRP composite properties and standard deviations

Fiber type	f_f (MPa)	E_f (GPa)	ε_{fu} (%)	t_f [a] (mm)
Carbon	2065 (80)	225 (12)	0.90 (0.07)	0.185
Aramid	2430 (260)	122 (16)	2.06 (0.11)	0.20

Note: Numbers in brackets indicate the standard deviation calculated from tests on three samples.
[a]t_f = dry fiber thickness of 1 layer.

The cyclic tests comprised five unloading/reloading cycles at increasing stress levels of 10 MPa, with the first cycle performed at a rate of 0.5 mm/min and the four subsequent cycles at 2 mm/min. During the tests, both local and global axial and lateral strains were monitored using strain gauges and laser distance sensors so as to determine the full stress–strain behavior of CRuC (Figure 1).

Table 1 and Figure 2 summarize the key results obtained from the cyclic tests, while Table 2 presents the mechanical properties of the unidirectional FRP jackets, as obtained from direct tensile coupon tests. The full details of the database, test methodology, and results are reported in 18. In Table 1 and Figure 2, K_{jn} is the normalized jacket stiffness [as defined in Equation (3)]; f_{cc} is the ultimate compressive strength of the cylinders; ε_{cc} and ε_{ccl} are the ultimate axial and lateral strains, respectively; f_{cr} and ε_{cr} are the critical stress and critical strain, respectively; f_0 is the intercept of the second (linear) part of the envelope stress–strain curve with the y-axis; and $E_{c,0}$ is the initial modulus of elasticity. The critical point (ε_{cr}, f_{cr}) defines the stress state coinciding with the activation of the confinement and marks the end of the initial linear behavior. In Table 1, the specimens are identified according to the number of confining layers (2 L, 3 L, or 4 L), the type of confining material (A = AFRP or C = CFRP), followed by a hyphen then loading type (C = cyclic or M = monotonic). For example, 3LA-C refers to cylinders wrapped with three layers of AFRP and subjected to cyclic loading. The key results listed in Table 1 are used to calibrate the cyclic model presented in Section 4 of this article.

2.1 | Cyclic versus monotonic behavior

Figure 3a–f compares typical stress–strain curves of the CRuC cylinders. In this figure, each plot includes the envelope curves of two monotonic tests and three cyclic tests for the same number of layers and type of confinement. The plots also show the "average" stress–strain curve of such monotonic and cyclic tests, as well as one full cyclic curve of a typical cylinder. Axial (compressive) and lateral (hoop tensile) strains are shown as positive and negative, respectively. From the analysis of Figure 3, it can be concluded that the loading regime had a negligible influence on the overall behavior of the specimens and the values of ultimate axial and lateral strain that could be mobilized for different confinement levels. This is consistent with existing research on confined conventional[27,28] or rubberized concrete,[18] where cyclic envelope stress–strain curves were shown to follow the stress–strain curves of monotonically loaded cylinders with similar levels of confinement, and direct comparisons were made.

The initial stiffness ($E_{c,0}$) of the envelope curves of CRuC up to the critical point (ε_{cr}, f_{cr}) is dominated by the

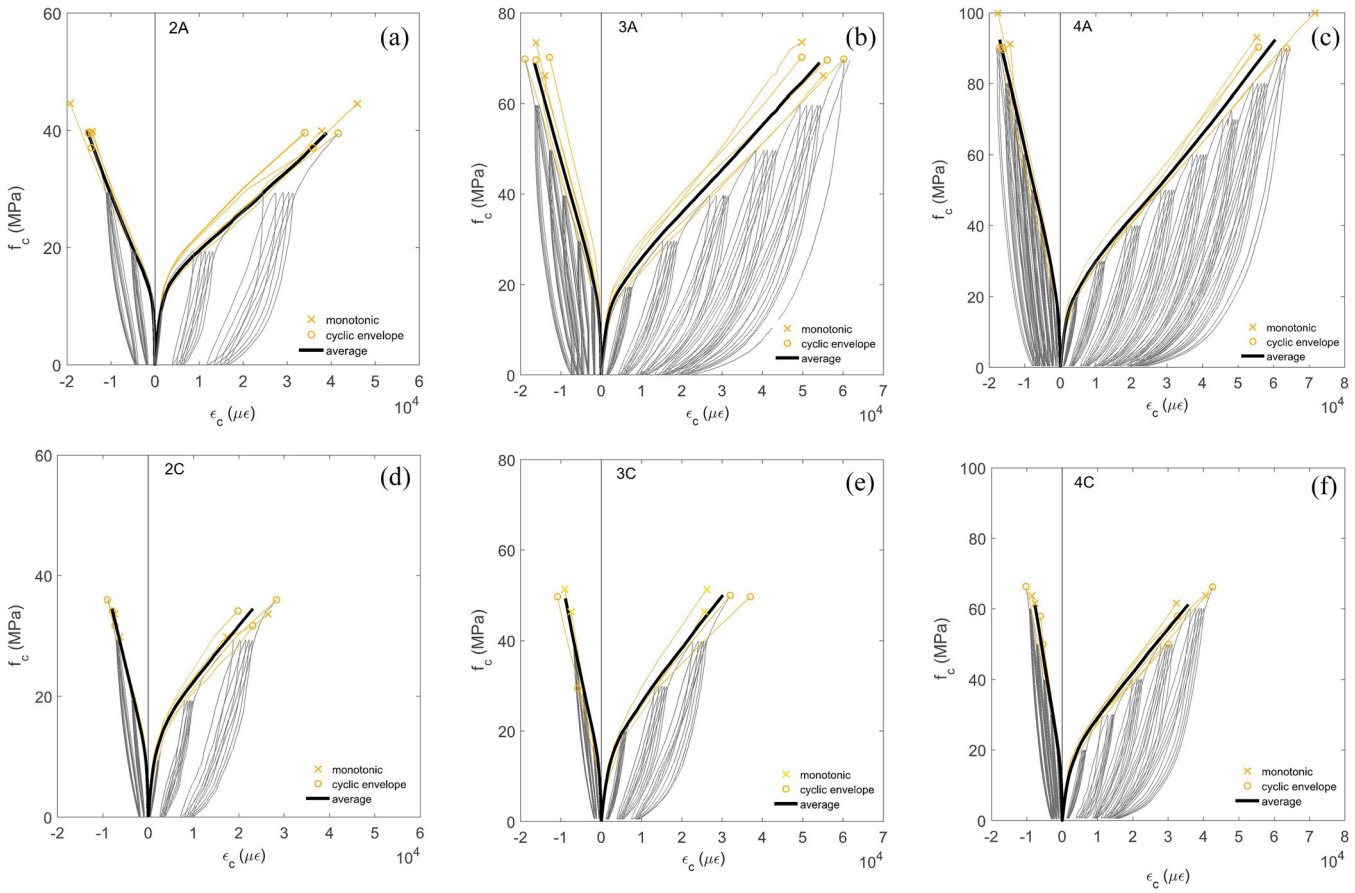

FIGURE 3 Typical stress–strain curves including average cyclic envelope and monotonic curves (a) 2LA, (b) 3LA, (c) 4LA, (d) 2LC, (e) 3LC, and (f) 4LC

linear elastic behavior of unconfined RuC. This initial linear behavior is then followed by a nonlinear transition zone and a second linear curve (gradient $E_{c,f}$), the latter being a function of the axial stiffness of the FRP jacket. At this last stage, the RuC is progressively crushing, which in turn increases the lateral expansion in the jacket.

All of the cylinders failed suddenly by rupture of the FRP jacket at a measured maximum lateral strain ε_{ccl} that was typically lower (Table 1) than the mean ultimate strains achieved in direct tensile (coupon) tests (see ε_{fu} in Table 2). For instance, the AFRP CRuC cylinders failed at ε_{ccl} values of around 70%–80% of ε_{fu}, whereas CFRP CRuC cylinders failed at ε_{ccl} values between 65% and 95% of ε_{fu}. These observations are consistent with previous research,[29,30] and the premature failure of the FRP can be attributed to (i) localized stress concentrations induced by nonhomogeneous deformations in the concrete or strain distribution in the FRP, (ii) FRP jacket curvature, (iii) axial loading of the FRP jacket, and (iv) slight misalignment of the fibers.

3 | A NEW CYCLIC MODEL FOR FRP CRUC

Although the behavior of conventional FRP-confined concrete has been extensively investigated and several constitutive models exist,[31–33] these models are unable to predict the behavior of CRuC due to its significantly higher strength and strain enhancement ratios, as well as delayed cracking when compared to conventional confined concrete.[11,17,34,35] Based on the test results discussed in the previous section, the key parameters that describe the uniaxial cyclic behavior of CRuC are identified in the following and a new model is proposed.

As shown in Figure 2, the cyclic axial stress–strain behavior of FRP CRuC can be fully described by its envelope (discontinuous line), and an unloading and reloading curve for each cycle. These curves are defined by the following parameters:

a. For the envelope: initial modulus of elasticity ($E_{c,0}$), slope of the second gradient of the curve ($E_{c,f}$), intersection of the second linear branch of the curve with the y-axis (f_0), ultimate stress (f_{cc}) and strain (ε_{cc}) values, and critical point (ε_{cr}, f_{cr}).
b. For each unloading curve: unloading point ($\varepsilon_{un,i}$, $f_{un,i}$) and plastic residual strain ($\varepsilon_{pl,i}$).
c. For each reloading curve: reloading secant modulus ($E_{re,i}$), inflection point ($\varepsilon_{inf,i}$, $f_{inf,i}$), stress at previous unloading strain ($f_{new,i}$), intersection of reloading curve with the envelope ($\varepsilon_{re,i}$, $f_{re,i}$), slope ($E_{c,i}$), and stress on the envelope curve ($f_{0,i}$) at a strain corresponding to $\varepsilon_{inf,i}$.

The following sections describe the above parameters and provide the equations to determine their values. It should be noted that the proposed model assumes that the unloading–reloading cycles are performed at stress levels beyond the initiation of unstable cracking (ε_{cr}, f_{cr}).

3.1 | Constitutive equations for the stress–strain envelope curve

Previous research showed that the high lateral expansion of RuC activates the confinement provided by the FRP jacket at lower axial stress levels than in conventional FRP-confined concrete.[11,18] This, in turn, delays the initiation of cracking in CRuC, leading to higher stress and strain enhancement ratios.

Research has also shown that, similar to FRP or steel-confined conventional concrete,[33,36] the monotonic and cyclic envelopes of stress–strain curves of FRP CRuC are similar up to failure.[18] Therefore, the equations proposed by the authors to describe the monotonic stress–strain curves of FRP CRuC[18] can be used to define the envelope curve of identical confined cylinders subjected to cyclic loading. Based on a regression analysis of test results from monotonically and cyclically loaded cylinders (test database described in Section 2[18]), Equations (1)–(6) were proposed to predict the ultimate stress and strain values of FRP CRuC with different confinement stiffnesses K_{jn}. The critical stress (f_{cr}) and axial strain at critical stress (ε_{cr}) can be determined using Equations (1) and (2), respectively.

$$f_{cr} = f_{co}\left(-6.5\times10^{-6}K_{jn}^2 + 5.8\times10^{-3}K_{jn} + 0.8\right) \quad (1)$$

$$\varepsilon_{cr} = -5.2\times10^{-9}K_{jn}^2 + 5.2\times10^{-6}K_{jn} + 0.0011 \quad (2)$$

where the jacket stiffness is defined by Equation (3):

$$K_{jn} = \beta\frac{2nt_f}{D}\frac{E_f}{f_{co}} \quad (3)$$

where β is an effectiveness factor that accounts for the lower effectiveness of CFRP confinement (relative to its jacket stiffness) when compared to AFRP confinement.

The ultimate stress (f_{cc}) and the confinement ratio (ω_w) for AFRP and CFRP CRuC can be determined using Equations (4) and (5), respectively, whereas the variation in ultimate strain as a function of the strength enhancement ratio is given by Equation (6). Full details on the derivation of Equations (1)–(6) are reported in reference [18].

$$f_{cc} = f_{cr}(1.06\omega_w + 1.25) \quad (4)$$

$$\omega_w = \beta \frac{4nt_f}{D} \frac{E_f \varepsilon_{ccl}}{f_{co}} \quad (5)$$

$$\varepsilon_{cc} = \varepsilon_{cr} \left(4.7 \left(\frac{f_{cc}}{f_{cr}} - 1.25 \right)^{1.2} + 1.5 \right) \quad (6)$$

Figure 4 compares the values of f_{cc}/f_{cr} for AFRP and CFRP CRuC as a function of the confinement ratio ω_w. It is shown that, for a given value of ω_w (assuming $\beta = 1$), the CFRP CRuC cylinders have a lower strength enhancement ratio than the AFRP CRuC cylinders, thus implying that the CFRP CRuC specimens were less "effectively" confined. This effect has been previously reported in various studies.[36–39] For instance, according to Dai et al.[37] in research on conventional confined concrete, a different confinement effectiveness was observed for AFRP and CFRP confinement, the latter of which was found to be around 30% less effective. Lim and Ozbakkaloglu[39] also observed that FRP effectiveness decreased as the fiber elastic modulus increased, while Teng et al.[38] reported variations in FRP effectiveness when comparing Glass FRP (GFRP) and CFRP conventional concrete confinement. This effect is attributed to differences in the physical and mechanical characteristics of the confining sheets, which may result in (i) different applied prestress during application due to differences in sheet flexibility; for example, the lower flexibility of CFRP sheets may result in less tight wrapping and more air voids; (ii) higher sheet transversal stiffness, leading to biaxial loading; (iii) fiber misalignment; and (iv) interlaminar stresses at FRP overlap. Nevertheless, due to the limited amount of research on AFRP-confined concrete, in general,[36,37,39] and on comparative studies for AFRP and CFRP confinement, in particular,[36,39] a different confinement effectiveness of CFRP and AFRP still remains a matter of further research. Based on the results of a regression analysis performed on the data obtained from this study, β was found to be 0.75 for CFRP CRuC and 1.0 for AFRP CRuC. Figure 4 shows that the predictions of Equation (4) match well the trend of both AFRP CRuC and CFRP CRuC cylinders (the latter adjusted by using β = 0.75 in Equation (5)).

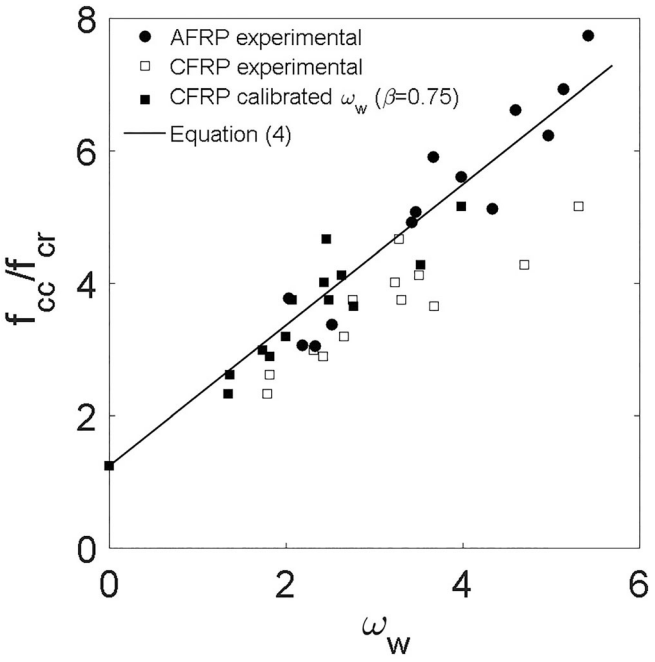

FIGURE 4 Effectiveness of confinement for AFRP and CFRP CRuC for different confinement ratios ω_w

The stress–strain model of the cyclic envelope curve builds on the model proposed by Samaan et al.[40] and further modified by Shao et al.[32] The envelope model by Shao et al.[32] was selected as it matches well the actual bilinear stress–strain response of FRP-confined concrete as well as its unique dilation properties. However, the model is modified to account for the different $E_{c,0}$, $E_{c,f}$, f_{cc}, ε_{cc}, and f_0. Accordingly, the model comprises an initial modulus of elasticity, a nonlinear transition zone, and a second linear slope. The stress–strain response is defined by

$$f_c = \frac{(E_{c,0} - E_{c,f})\varepsilon_c}{\left[1 + \left(\frac{(E_{c,0} - E_{c,f})\varepsilon_c}{f_0}\right)^{n_0}\right]^{1/n_0}} + E_{c,f}\varepsilon_c \quad (7)$$

where n_0 is a shape parameter that defines the curvature of the transition zone, and f_0 is the intercept of the second linear branch of the curve with the y-axis (see Figure 2).

The value of n_0 was found to be 1.5, and a similar value was indicated by Shao et al.[32] for FRP-confined conventional concrete. The adoption of a value $n_0 = 1.5$ is reasonable as the shape of the transition zone in FRP CRuC is similar to that observed in FRP-confined conventional concrete.[32] Moreover, the changes due to delayed cracking and the increased gradient in the second part of the curve could be captured adequately by the calibrated $E_{c,f}$ and f_0 values.

The values of $E_{c,f}$ and f_0 can be determined as a function of K_{jn} according to Equations (8) and (9), respectively, which were derived by performing a regression analysis on the experimental data:

$$E_{c,f} = -0.0095(K_{jn})^2 + 6.85(K_{jn}) \quad (8)$$

$$f_0 = f_{co}\left(-7.35 * 10^{-6}(K_{jn})^2 + 6.9 * 10^{-3}(K_{jn}) + 1\right) \quad (9)$$

Figure 5 compares the average experimental stress–strain curves for the cylinders examined in this study (see

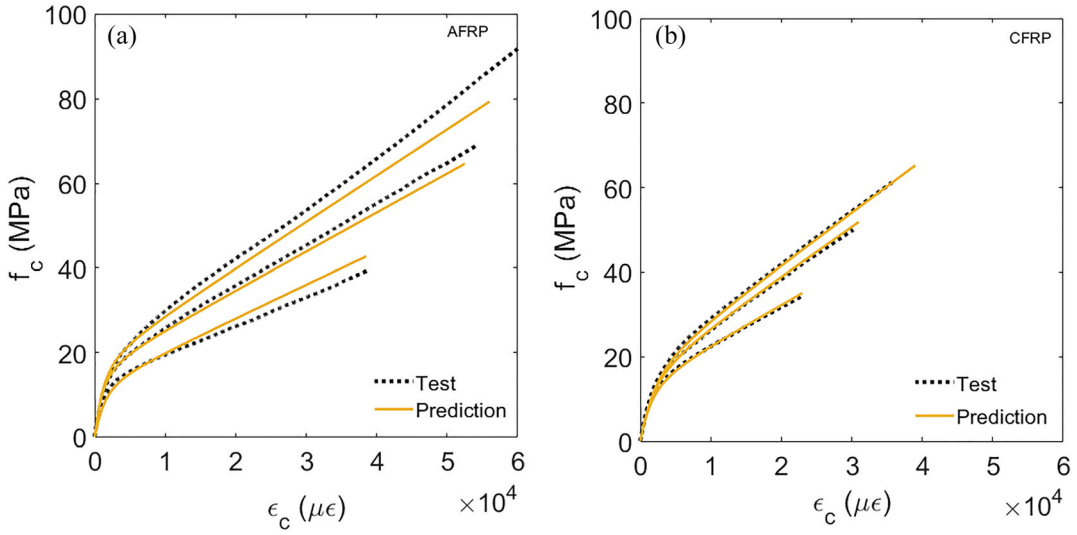

FIGURE 5 Predictions vs. experimental envelope curves of CRuC cylinders confined with (a) AFRP and (b) CFRP jackets

Table 2) and the predictions from Equations (1)–(9). As it can be seen, the proposed model approximates reasonably well the experimental stress–strain curves, albeit with minor differences due to the difficulty of capturing the variability in the data obtained from the two sets of cylinders confined with AFRP or CFRP at different levels of confinement. As shown in Figure 5a, the highest discrepancy between the predicted and "average" test result corresponds to cylinders with 4L AFRP. Such variation is not observed for the other specimens (e.g., 2LC, 3LC, 2LA) where the predicted axial strains are very close to the average test results. While some experimental strains seem to be much larger than the predicted strains, as a percentage, the predictions are within the variability obtained from the test data. For example, based on the standard deviation shown in Table 1, it can be seen that the axial strain in cylinders 4LA ranges between 5.3% and 7.4%. The predicted strain for 4L AFRP is 5.6%, which is within the range.

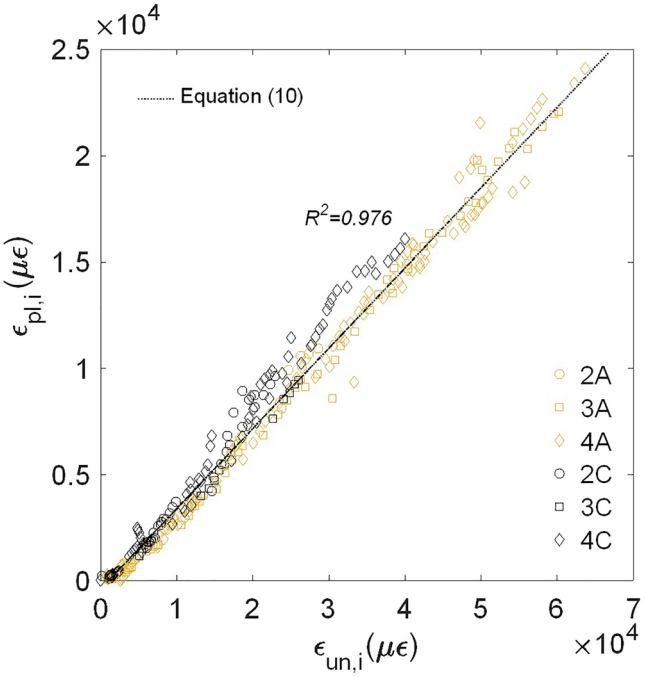

FIGURE 6 Relationship between plastic and unloading strains of tested cylinders

3.2 | Plastic, unloading, and reloading strains

In line with previous studies,[33,36,41] the relationship between the unloading ($\varepsilon_{un,i}$) and plastic ($\varepsilon_{pl,i}$) strains for the CRuC specimens examined in this study was not found to be significantly affected by the type of confining material or number of confining layers (Figure 6), and it can be approximated well by the linear model in Equation (10):

$$\varepsilon_{pl,i} = 4 \cdot (0.095\varepsilon_{un,i} - 0.0001), \ for\, \varepsilon_{un,i} > \varepsilon_{cr} \qquad (10)$$

Figure 7 presents the relationship between the reloading strain ($\varepsilon_{re,i}$) and unloading strain ($\varepsilon_{un,i}$). The reloading strain, $\varepsilon_{re,i}$, was determined as the intersection of the reloading curve of the fifth and final cycle in each set of cycles with the envelope curve. The experimental results indicate that $\varepsilon_{re,i}$ also increases linearly with $\varepsilon_{un,i}$ of the corresponding cycle. Accordingly, $\varepsilon_{re,i}$ can be predicted for $\varepsilon_{un,i} > \varepsilon_{cr}$ using Equation (11). The value $\varepsilon_{re,i}$ can then be used to determine the reloading stress ($f_{re,i}$) using the stress–strain envelope defined by Equation (7).

$$\varepsilon_{re,i} = 1.06\varepsilon_{un,i} + 0.002, \ for\, \varepsilon_{un,i} > \varepsilon_{cr} \qquad (11)$$

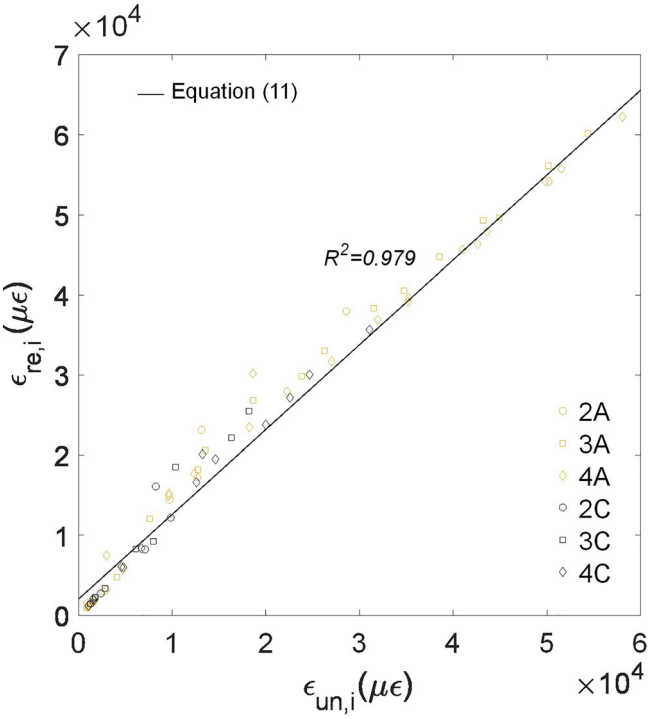

FIGURE 7 Relationship between reloading and unloading strains of tested cylinders

3.3 | Unloading curve

The unloading curve is defined by (a) the unloading strain and stress on the envelope curve, i.e., point ($\varepsilon_{un,i}$, $f_{un,i}$) in Figure 2 and (b) the residual plastic strain ($\varepsilon_{pl,i}$) at zero stress, i.e., point ($\varepsilon_{pl,i}$, 0). Figure 8 shows typical unloading curves for cylinders confined with four layers of AFRP/CFRP. With the exception of unloading cycles that were performed before reaching the critical stress, the unloading curves are nonlinear and are characterized by an initial stiffness that increases with increasing unloading strains ($\varepsilon_{un,i}$). This is consistent with previous findings[33,42,43] and indicates the accumulation of non-recoverable damage in the concrete. Indeed, the presence of rubber particles and the large strains developed in CRuC (>5%[18]) lead to complex damage accumulation effects, which are difficult to capture by conventional confinement models.

The polynomial function proposed by Shao et al.[32] (Equation 12) was adopted to model the unloading curves of the CRuC cylinders presented in this study.

$$f_c = \frac{(1-x)^m}{(1+kx)^{n_{un,i}}} \cdot f_{un,i} \tag{12}$$

where

$$x = \frac{\varepsilon_c - \varepsilon_{un,i}}{\varepsilon_{pl,i} - \varepsilon_{un,i}} \tag{13}$$

and $n_{un,i}$, m, and k are empirically calibrated shape parameters.

The optimal values of $n_{un,i}$, m, and k for each set of unloading curves were found by implementing a single-objective genetic algorithm,[44] which aimed at minimizing the difference in area under the experimental and predicted curves. Based on this optimization, a value of 1 was found suitable for both m and k. To account for the effect of the increasing cyclic stress level on the curvature of the unloading curve, the value $n_{un,i}$ was set to vary with the change in the envelope $\varepsilon_{un,i}$, as shown in Equation (14).

$$n_{un,i} = 16(\varepsilon_{un,i})^{0.5} \tag{14}$$

Figure 8 shows the experimental unloading curves obtained for CRuC cylinders confined with four layers of AFRP and CFRP, along with the analytical curves predicted using Equation (12) and the estimated values of $\varepsilon_{pl,i}$ and $n_{un,i}$ according to Equations (10) and (14), respectively. It is evident that the adopted model approximates well the test results over the entire load history.

3.4 | Cyclic stress and stiffness degradation

The stress degradation ($f_{\text{new},i}/f_{un,i}$) of the cylinders after a cycle performed at a given stress level ($f_{un,i}$), which is calculated as the ratio of the stress at the preceding unloading strain ($\varepsilon_{un,i}$) achieved upon reloading ($f_{\text{new},i}$) and the preceding unloading stress ($f_{un,i}$), is shown in Figure 9.

As evident in Figure 9, the application of cyclic loading has a minor effect on stress degradation, regardless of the number of confining layers and type of FRP material. In general, while a rapid degradation is observed following load cycles performed at low strain levels (up to $\varepsilon_{un,i} = 0.01$), the maximum mean cyclic stress degradation is only about 8% ($f_{\text{new},i}/f_{un,i} = 0.92$). A slight increase in the ratio $f_{\text{new},i}/f_{un,i}$ was observed in some tests at very large unloading strains ($\varepsilon_{un,i} > 0.03$). This can be attributed to the increased material packing at higher stress and confinement levels, which in turn increases the amount of stress being transferred between the aggregates through direct bearing. Further research is needed to capture this phenomenon and to understand the effect of confining material, loading history (e.g., cyclic fatigue) as well as partial unloading/reloading on stress degradation.

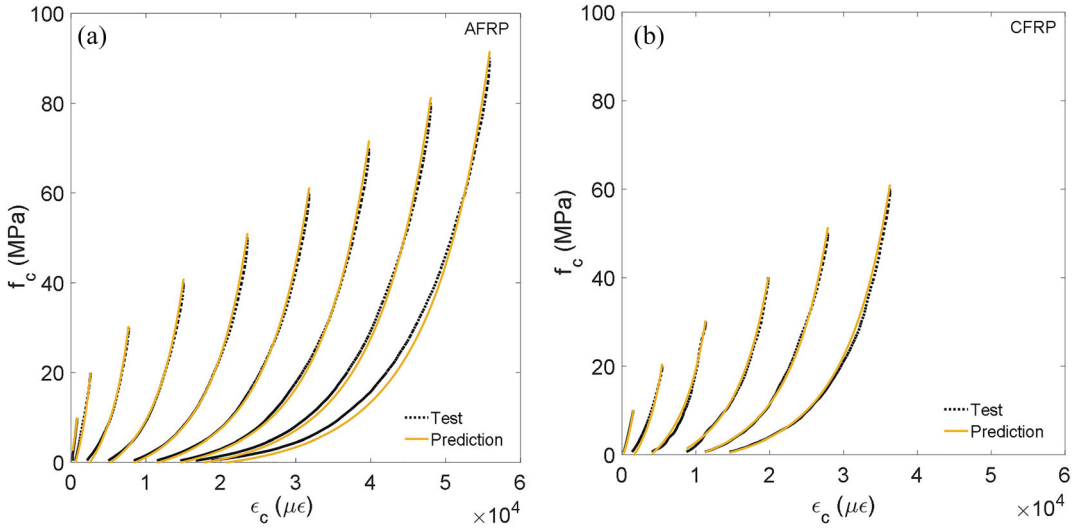

FIGURE 8 Predictions of unloading curves for RuC specimens confined with four layers of (a) AFRP and (b) CFRP

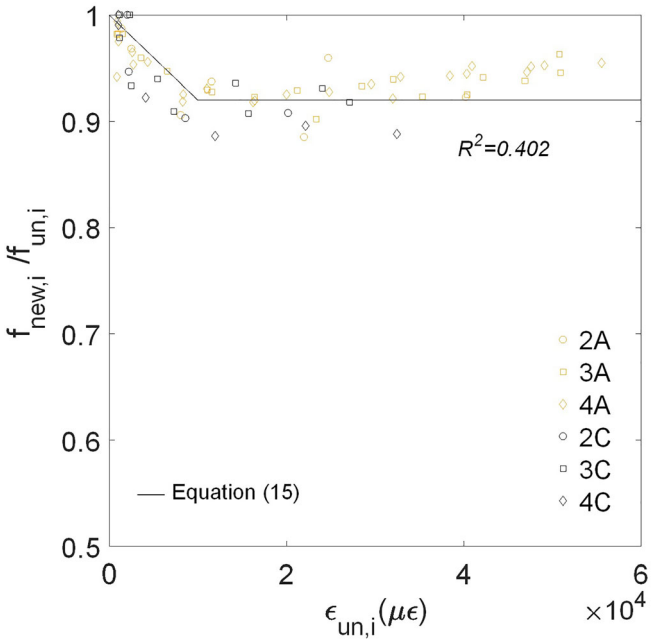

FIGURE 9 Stress degradation ($f_{\text{new},i}/f_{un,i}$) due to cyclic loading

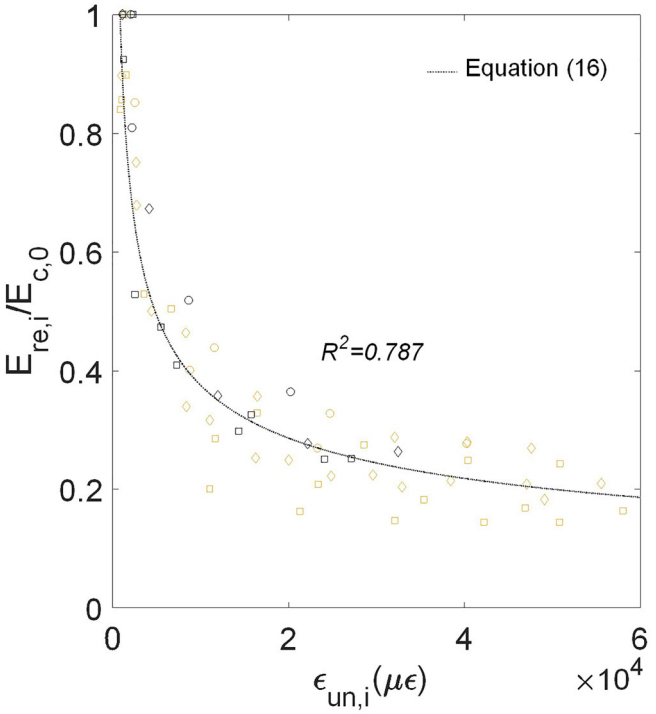

FIGURE 10 Stiffness degradation at increasing $\varepsilon_{un,i}$

Based on the level of damage achieved in the specimens (reflected in $\varepsilon_{un,i}$), and similar to previous work by Lam and Teng[33] and Yu et al.,[45] the cyclic stress degradation can be reasonably approximated by the bilinear relationship shown in Figure 9 and described by Equation (15):

$$\frac{f_{\text{new},i}}{f_{un,i}} = \begin{cases} 1-8(\varepsilon_{un,i}) & for\ \varepsilon_{un,i} < 0.01 \\ 0.92 & for\ \varepsilon_{un,i} > 0.01 \end{cases} \quad (15)$$

Figure 10 shows the evolution of stiffness degradation ($E_{re,i}/E_{c,0}$) at increasing $\varepsilon_{un,i}$ for both AFRP and CFRP CRuC specimens. The stiffness of each reloading curve ($E_{re,i}$) is taken as the secant stiffness at the point ($\varepsilon_{un,i}$, $f_{\text{new},i}$) shown in Figure 2.

All specimens exhibit a significant stiffness degradation up to $\varepsilon_{un,i} = 0.01$, after which the rate of degradation decreases substantially and stabilizes at around 20% of the initial stiffness of the cylinder ($E_{c,0}$). The type and number of FRP layers seem to have negligible influence on the stiffness degradation, which was mainly controlled by the axial strain imposed on the cylinders ($\varepsilon_{un,i}$). Based

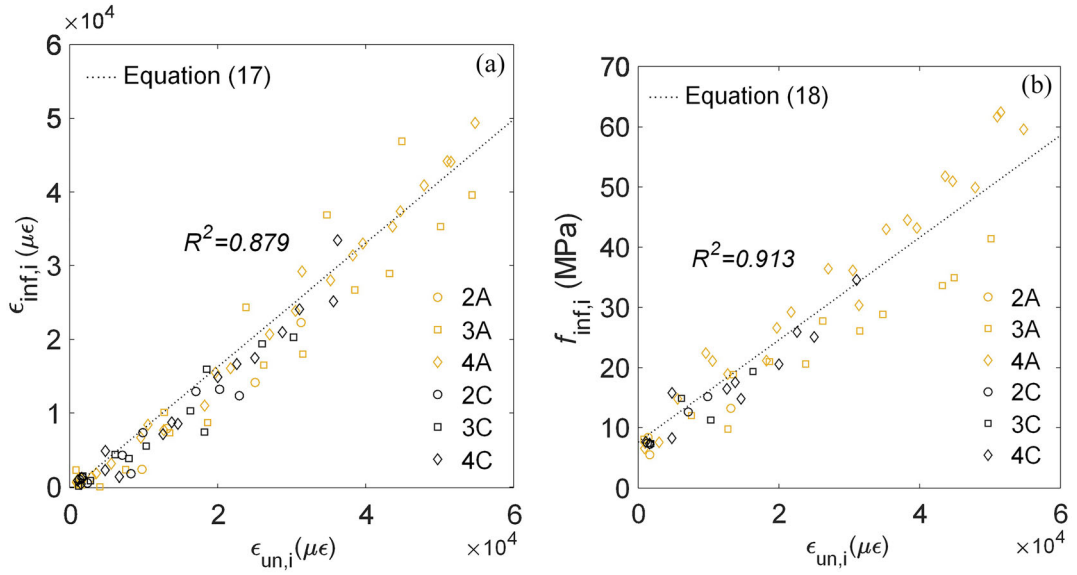

FIGURE 11 Inflection (a) strain $\varepsilon_{\text{inf},i}$ and (b) stress $f_{\text{inf},i}$ as function of $\varepsilon_{un,i}$

on the results of a regression analysis performed on the data shown in Figure 10, the stiffness degradation after a cycle performed at a stress level corresponding to $\varepsilon_{un,i}$ can be estimated using Equation 16 (where $\varepsilon_{un,i}$ is in microstrain).

$$E_{re,i} = 13.8 \cdot E_{c,0} \left(\frac{1}{\varepsilon_{un,i}} \right)^{0.4} \tag{16}$$

3.5 | Reloading curve

While a linear relationship has been shown to adequately model the reloading curves of FRP-confined conventional concrete,[42,46] CRuC exhibits a highly nonlinear behavior, particularly at high strain levels (Figure 3). The reloading curves are characterized by a soft initial part, which stiffens at increasing strain levels (strain stiffening), followed by a strain hardening phase. The initial strain stiffening behavior of the reloading curve can be attributed to the closure of cracks (which are wider at higher strain levels[32]) and to the mechanical properties of the rubber particles.[47]

The strain ($\varepsilon_{\text{inf},i}$) and corresponding stress ($f_{\text{inf},i}$) values of the point at which the behavior changes from strain stiffening to hardening (inflection point) were found to increase linearly with $\varepsilon_{un,i}$, as shown in Figure 11a–b.

Based on a regression analysis of the data in Figure 11a–b, the coordinates of the inflection point ($\varepsilon_{\text{inf},i}$, $f_{\text{inf},i}$) can be calculated using Equations 17 and 18.

$$\varepsilon_{\text{inf},i} = 0.94\varepsilon_{un,i} - 5.2 \times 10^{-4}, \quad for\ \varepsilon_{un,i} > \varepsilon_{cr} \tag{17}$$

$$f_{\text{inf},i} = 1040\varepsilon_{un,i} + 7.6, \quad for\ \varepsilon_{un,i} > \varepsilon_{cr} \tag{18}$$

The models proposed to describe the strain stiffening phase (from ($\varepsilon_{pl,i}$,0) to ($\varepsilon_{\text{inf},i}$, $f_{\text{inf},i}$)) and the strain hardening phase (from ($\varepsilon_{\text{inf},i}$, $f_{\text{inf},i}$) to ($\varepsilon_{re,i}$, $f_{re,i}$)) are presented in the following sections.

3.5.1 | Reloading stage 1: Strain stiffening

The strain stiffening (stage 1) of the reloading curve was found to be accurately modeled by the polynomial function proposed by Shao et al.[32] but with different boundary conditions for f_c and x so as to limit its domain to ($\varepsilon_{\text{inf},i}$, $f_{\text{inf},i}$):

$$f_c = \frac{(1-x)^m}{(1+kx)^{n_{re,i}}} \cdot f_{\text{inf},i} \tag{19}$$

$$x = \frac{\varepsilon_c - \varepsilon_{\text{inf},i}}{\varepsilon_{pl,i} - \varepsilon_{\text{inf},i}} \tag{20}$$

The shape parameters (m, $n_{re,i}$, and k) in Equations (19) and (20) were calibrated using a single-objective genetic algorithm, and both m and k were found to be equal to 1. As discussed in Section 3.3, the same values of m and k were also found suitable to describe the unloading path. The parameter $n_{re,i}$ was found to be a function of the envelope $\varepsilon_{un,i}$ and can be defined as shown in Equation (21).

$$n_{re,i} = 55(\varepsilon_{un,i})^{1.3} \tag{21}$$

3.5.2 | Reloading stage 2: Strain hardening

The strain hardening phase of the reloading path (stage 2) can be described by the same parabolic function defined by Equation (7) but using parameters that are cycle-dependent (Equation 22):

$$f_c = \frac{\left(E_{c,i} - E_{c,f}\right)\varepsilon_c}{\left[1 + \left(\frac{\left(E_{c,i} - E_{c,f}\right)\varepsilon_c}{f_{0,i}}\right)^{n_{0,i}}\right]^{1/n_{0,i}}} + E_{c,f}\varepsilon_c \quad (22)$$

where $E_{c,i}$ is the initial elastic modulus of the second part of the reloading curve, as estimated by the slope ($df_c/d\varepsilon_c$) of the stiffening curve at ($\varepsilon_{\text{inf},i}$, $f_{\text{inf},i}$) and Equation (23); $f_{0,i}$ is the intersection point of a vertical line at ($\varepsilon_{\text{inf},i}$, $f_{\text{inf},i}$) with the envelope curve; and $n_{0,i}$ is the curvature of the transition zone between ($\varepsilon_{un,i}$, $f_{\text{new},i}$) and ($\varepsilon_{re,i}$, $f_{re,i}$). The intersection of the reloading curve with the envelope ($\varepsilon_{re,i}$, $f_{re,i}$) was determined through a regression analysis of the experimental data. $E_{c,f}$, which denotes the slope of the linear portion of the envelope curve, can be determined as a function of the confining stiffness using Equation (8).

$$E_{c,i} = \frac{1 + n_{re,i}}{\varepsilon_{\text{inf},i} - \varepsilon_{pl,i}} f_{\text{inf},i} \quad (23)$$

Based on a regression analysis of the experimental data, $f_{0,i}$ and $n_{0,i}$ can be estimated using Equations (24) and (25), respectively.

$$f_{0,i} = 0.25\left(K_{jn}\right)\varepsilon_{un,i} + 8.1 \quad (24)$$

$$n_{0,i} = 2132\left(\varepsilon_{un,i}\right)^2 - 255\varepsilon_{un,i} + 8.5 \quad (25)$$

where all the variables are as defined before.

Figure 12a,b shows the full experimental reloading path for cylinders confined with four layers of AFRP or CFRP, respectively, along with the stress–strain behavior predicted through the implementation of the proposed model (Equations (1)–(25)). As can be seen, the proposed relationships are able to capture accurately the experimental response of the tested specimens over the entire load history.

4 | MODEL PREDICTION

Figure 13a–f compares the analytical predictions obtained from the implementation of the model developed above (Equations (1) to (25)) with a typical experimental response of cylinders confined with two, three, or four layers of AFRP or CFRP over the entire loading history. Overall, the proposed model captures reasonably well the experimental data and provides reliable estimates of the effect of subsequent load cycles on the degradation of the mechanical properties of CRuC. The discrepancies between the experimental and predicted curves observed in CRuC confined with two layers of AFRP (Figure 13a) can be attributed to the difficulty of fully capturing the variability associated with the use of different confining configurations and materials with a single unified model.

It should be noted that the proposed model is applicable to high rubber volumetric ratios, such as those used in this study (i.e., replacing 60% of the total aggregate

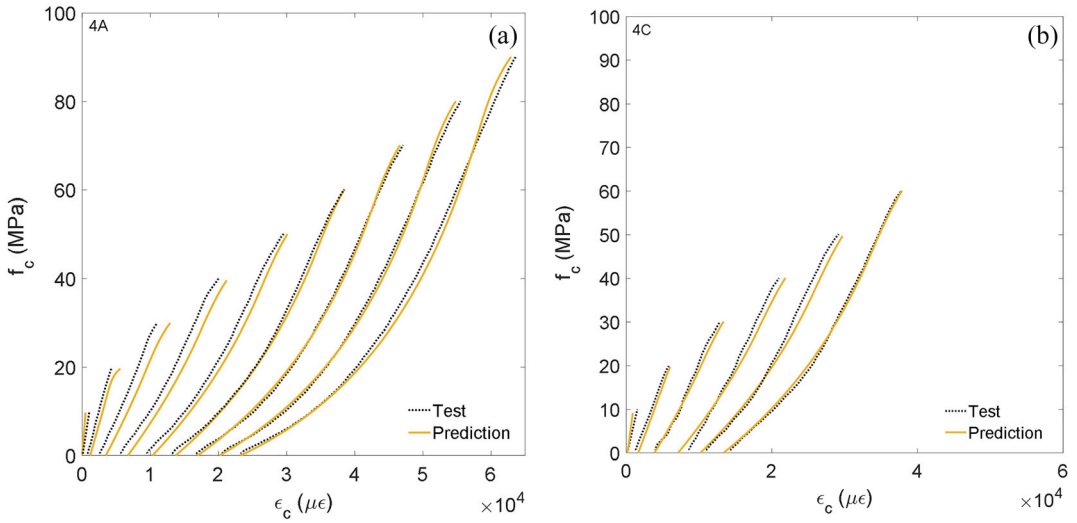

FIGURE 12 Comparison between test results and predictions of reloading curves for RuC specimens confined with four layers of (a) AFRP and (b) CFRP sheets

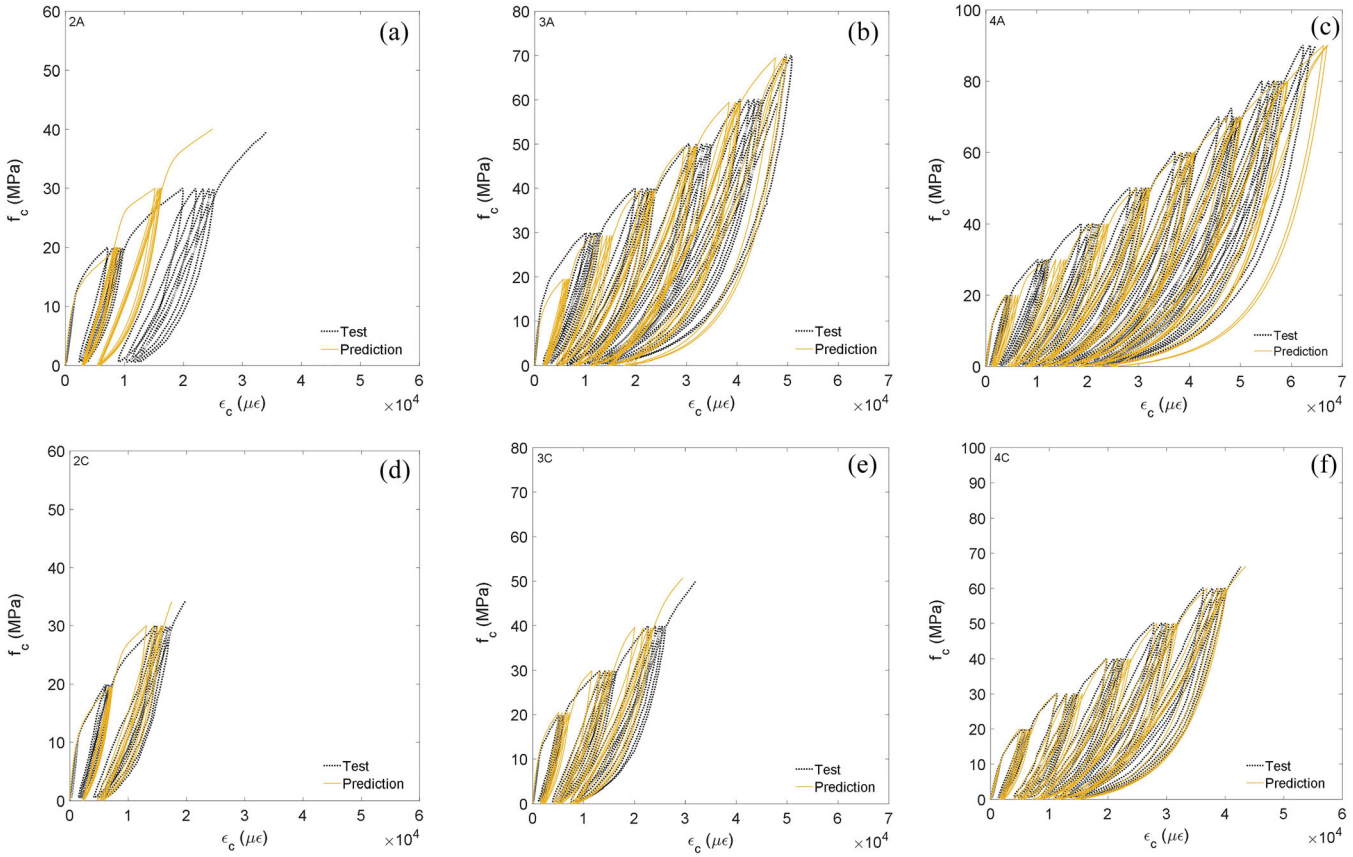

FIGURE 13 Predictions of cyclic behavior of RuC specimens confined with two, three, or four layers of AFRP (a, b, c, respectively) or identical layers of CFRP sheets (d, e, f, respectively)

content), as the volumetric ratio of rubber can affect concrete dilation characteristics and the initiation of micro-cracks.[18] It must also be noted that, to date, research on FRP CRuC with high rubber contents is not available in the literature and therefore the model has only been validated against a small dataset of experimental results. Future research should assess the validity of the model using other experimental datasets (when available) and extend the applicability of the model to other rubber contents and confining materials (e.g., Glass and/or Basalt FRP). Other parameters to investigate include the effect of concrete strength and mix proportions, rubber properties, particle size distribution, and specimen size. Further work is also needed to assess the accuracy of the model when different load protocols are used (e.g., cyclic fatigue, partial unloading/reloading). Finally, further research also needs to evaluate other models in the literature[33,37,43,48,49] to extend the work in this study and previous research[18] so as to develop versatile analytical-oriented constitutive models (with lateral-to-axial strain relationships) defining the full cyclic constitutive response of FRP CRuC.

5 | CONCLUSIONS

This study proposed a new design-oriented constitutive model to predict the cyclic behavior of rubberized concrete cylinders confined with FRP sheets. The model was calibrated using test results from 18 confined rubberized concrete (CRuC) cylinders with high volume of tyre rubber (60% total aggregate replacement) subjected to cyclic uniaxial compressive loading. The parameters investigated included (i) type of confining material (AFRP or CFRP sheets) and (ii) number of FRP layers (two, three, or four layers). Based on the test results and analyses presented in this study, the following conclusions are drawn:

1. The envelope stress–strain response of cyclically loaded CRuC cylinders can be described adequately by a bilinear equation previously proposed for conventional FRP-confined concrete, accounting for the unique properties of CRuC, such as higher confinement effectiveness and earlier activation of the FRP confinement.
2. The nonlinear unloading stress–strain relationship can be modeled accurately by calibrating the

predictive equation by Shao et al.[32] and by expressing the shape parameter ($n_{un,i}$) as a function of the unloading strain ($\varepsilon_{un,i}$).
3. The reloading curve is characterized by an initial strain stiffening phase followed by a strain hardening phase. The proposed model captures both stages of the reloading curve through the use of cycle-dependent parameters over the entire load history.
4. The proposed cyclic model predicts the behavior of AFRP/CFRP CRuC with reasonable accuracy. However, future research should investigate the validity of the model against experimental data of CRuC with different rubber contents and different types and levels of confinement, once such data are available.

ACKNOWLEDGMENTS

The research leading to these results has received funding from the European Union Seventh Framework Programme [FP7/2007-2013] under grant agreement n° 603722 and the European Union's Horizon 2020 research and innovation program under the Marie Sklodowska-Curie grant agreement n° 658248 and grant agreement n° 101029972. The authors also thank Richard Morris from Tarmac UK for providing the Portland Limestone Cement (CEM II 52.5 N). The AFRP and CFRP systems were kindly provided by S&P (Switzerland) and Fyfe Europe S.A., respectively.

DATA AVAILABILITY STATEMENT

The data that support the findings of this study are available from the corresponding author upon reasonable request.

NOMENCLATURE

D cylinder diameter
$E_{c,0}$ concrete initial modulus of elasticity
$E_{c,f}$ gradient of the linear portion of the envelope curve (i.e., after the critical point)
E_f tensile modulus of elasticity of the FRP fibers
$E_{c,i}$ initial gradient of the softening part of each reloading curve
$E_{re,i}$ reloading secant modulus
K_{jn} normalized confining stiffness
n number of FRP confining layers
n_0 shape parameter that defines the curvature of the transition zone in the envelope curve
$n_{0,i}$ shape parameter that defines the curvature of the softening part of the reloading curve
$n_{re,i}$ shape parameter that defines the curvature of the hardening part of the reloading curve
$n_{un,i}$ shape parameter that defines the curvature of the unloading curve
f_0 intercept of the second (linear) part of the envelope curve with the y-axis
$f_{0,i}$ intercept of the vertical at (ε_{inf}, f_{inf}) with the envelope curve for each reloading curve
f_c axial compressive stress in confined or unconfined concrete
f_{cc} compressive strength of confined concrete
f_{co} unconfined concrete compressive strength
f_{cr} critical stress
f_f tensile strength of the FRP coupon
$f_{\text{inf},i}$ axial compressive stress at the inflection point of each reloading curve
$f_{\text{new},i}$ reloading stress at $\varepsilon_{un,i}$ of the corresponding cycle
$f_{re,i}$ axial stress upon intersection of reloading curve with the envelope
$f_{un,i}$ axial stress at unloading
t_{f} dry fiber thickness of FRP sheet
β confinement effectiveness factor
ε_c axial compressive strain in confined or unconfined concrete
ε_{cc} confined concrete ultimate axial strain
ε_{ccl} confined concrete ultimate hoop strain
ε_{co} axial strain at peak stress in unconfined confined
ε_{cr} axial strain at critical stress
$\varepsilon_{\text{inf},i}$ axial compressive strain at the inflection point of each reloading curve
ε_{fu} ultimate elongation of FRP coupons (in direct tension)
$\varepsilon_{pl,i}$ residual plastic strain upon full unloading
$\varepsilon_{re,i}$ axial strain upon intersection of each reloading curve with the envelope
$\varepsilon_{un,i}$ axial strain at unloading
ω_w mechanical volumetric confinement ratio

ORCID

Samar Raffoul https://orcid.org/0000-0003-2261-206X
Maurizio Guadagnini https://orcid.org/0000-0003-2551-2187

REFERENCES

1. Ismail M, Hassan A. Ductility and cracking behavior of reinforced self-consolidating rubberized concrete beams. J Mater Civ Eng. 2016;29(1):4016174. https://doi.org/10.1061/(ASCE)MT.1943-5533.0001699
2. Jain A, Siddique S, Gupta T, Jain S, Sharma RK, Chaudhary S. Evaluation of concrete containing waste plastic shredded fibers: ductility propreties. Struct Concr. 2021;22:566–75. https://doi.org/10.1002/suco.201900512
3. Son KS, Hajirasouliha I, Pilakoutas K. Strength and deformability of waste tyre rubber-filled reinforced concrete columns. Construct Build Mater. 2011;25:218–26.

4. Zheng L, Huo XS, Yuan Y. Strength, modulus of elasticity, and brittleness index of rubberized concrete. J Mater Civ Eng. 2008; 20:692–9.
5. Benazzouk A, Douzane O, Langlet T, Mezreb K, Roucoult JM, Quéneudec M. Physico-mechanical properties and water absorption of cement composite containing shredded rubber wastes. Cem Concr Compos. 2007;29:732–40.
6. Flores-Medina D, Medina NF, Hernández-Olivares F. Static mechanical properties of waste rests of recycled rubber and high quality recycled rubber from crumbed tyres used as aggregate in dry consistency concretes. Mater Struct. 2014;47:1185–93.
7. Pham TM, Renaud N, Pang VL, Shi F, Hao H, Chen W. Effect of rubber aggregate size on static and dynamic compressive properties of rubberized concrete. Struct Concr. 2021;1–13. https://doi.org/10.1002/suco.202100281
8. Güneyisi E, Gesoğlu M, Özturan T. Properties of rubberized concretes containing silica fume. Cem Concr Res. 2004;34: 2309–17.
9. Eldin NN, Senouci AB. Measurement and prediction of the strength of rubberized concrete. Cem Concr Compos. 1994;16: 287–98.
10. Raffoul S, Garcia R, Pilakoutas K, Guadagnini M, Medina NF. Optimisation of rubberised concrete with high rubber content: an experimental investigation. Construct Build Mater. 2016; 124:391–404. https://doi.org/10.1016/j.conbuildmat.2016.07.054
11. Li G, Pang SS, Ibekwe SI. FRP tube encased rubberized concrete cylinders. Mater Struct. 2011;44:233–43.
12. Youssf O, ElGawady MA, Mills JE, Ma X. An experimental investigation of crumb rubber concrete confined by fibre reinforced polymer tubes. Construct Build Mater. 2014;53:522–32.
13. Duarte APC, Silva BA, Silvestre N, De Brito J, Júlio E, Castro JM. Experimental study on short rubberized concrete-filled steel tubes under cyclic loading. Compos Struct. 2016; 136:394–404.
14. Duarte APC, Silva BA, Silvestre N, De Brito J, Júlio E, Castro JM. Tests and design of short steel tubes filled with rubberised concrete. Eng Struct. 2016;112:274–86.
15. Moustafa A, ElGawady MA. Strain rate effect on properties of rubberized concrete confined with glass fiber–reinforced polymers. J Compos Constr. 2016;20:4016014.
16. Lam L, Teng JG. Design-oriented stress–strain model for FRP-confined concrete. Construct Build Mater. 2003;17:471–89.
17. Raffoul S, Garcia R, Escolano-Margarit D, Guadagnini M, Hajirasouliha I, Pilakoutas K. Behaviour of unconfined and FRP-confined rubberised concrete in axial compression. Construct Build Mater. 2017;147:388–97. https://doi.org/10.1016/j.conbuildmat.2017.04.175
18. Raffoul S, Escolano-Margarit D, Garcia R, Guadagnini M, Pilakoutas K. Constitutive model for rubberized concrete passively confined with FRP laminates. J Compos Constr. 2019; 23(9):04019044. https://doi.org/10.1061/(ASCE)CC.1943-5614.0000972
19. Lai MH, Liang YW, Wang Q, Ren FM, Chen MT, Ho JCM. A stress-path dependent stress-strain model for FRP-confined concrete. Eng Struct. 2020;203:109824. https://doi.org/10.1016/j.engstruct.2019.109824
20. Ho JCM, Ou XL, Chen MT, Wang Q, Lai MH. A path dependent constitutive model for CFFT column. Eng Struct. 2020; 210:110367. https://doi.org/10.1016/j.engstruct.2020.110367
21. CORDIS. Innovative reuse of all tyre components in concrete. https://cordis.europa.eu/project/rcn/111538/factsheet/en (2017). Accessed 31 March 2022.
22. Wong HHC, Kwan AKH. Packing density of cementitious materials: part 1—measurement using a wet packing method. Mater Struct. 2008;41:689–701.
23. Kwan AKH, Wong HHC. Packing density of cementitious materials; part 2—packing and flor of OPC + PFA + CSF. Mater Struct. 2008;41:773–84.
24. Kwan AKH, Chen J-J, Fung WWS. Effects of superplasticiser on rheology and cohesiveness of CSF cement paste. Adv Cem Res. 2012;24(3):125–37. https://doi.org/10.1680/adcr.10.00020
25. Maybury J, Ho JCM, Binhowimal SAM. Fillers to lessen shear thickening of cement powder paste. Construct Build Mater. 2017; 142:268–79. https://doi.org/10.1016/j.conbuildmat.2017.03.076
26. Lai M, Hanzic L, Ho JCM. Fillers to improve passing ability of concrete. Struct Concr. 2019;20(1):185–97. https://doi.org/10.1002/suco.201800047
27. Osorio E, Bairan JM, Mari AR. Lateral behavior of concrete under uniaxial compressive cyclic loading. Mater Struct. 2013; 46(5):709–24. https://doi.org/10.1617/s11527-012-9928-9
28. Rousakis TC, Athanasios KI. Adequately FRP-confined reinforced concrete columns under axial compressive monotonic or cyclic loading. Mater Struct. 2012;45(7):957–75. https://doi.org/10.1617/s11527-011-9810-1
29. Matthys S, Toutanji H, Taerwe L. Stress–strain behavior of large-scale circular columns confined with FRP composites. J Struct Eng. 2006;132:123–33. https://doi.org/10.1061/(ASCE)0733-9445(2006)132:1(123)
30. Lam L, Teng JG. Ultimate condition of fiber reinforced polymer-confined concrete. J Compos Constr. 2004;8: 539–48.
31. Mander JB, Priestley MJN, Park R. Theoretical stress strain model for confined concrete. J Struct Eng. 1988;114:1804–25. https://doi.org/10.1061/(ASCE)0733-9445(1988)114:8(1804)
32. Shao Y, Zhu Z, Mirmiran A. Cyclic modeling of FRP-confined concrete with improved ductility. Cem Concr Compos. 2006;28:959–68. https://doi.org/10.1016/j.cemconcomp.2006.07.009
33. Lam L, Teng JG. Stress-strain model for FRP-confined concrete under cyclic axial compression. Eng Struct. 2009;31:308–21. https://doi.org/10.1016/j.engstruct.2008.08.014
34. Wang Z, Chen L, Guadagnini M, Pilakoutas K. Shear behavior model for FRP-confined and unconfinred rubberized concrete. J Compos Constr. 2019;23:04019039. https://doi.org/10.1061/(ASCE)CC.1943-5614.0000962
35. Bompa D, Elghazouli AY. Stress-strain response and practical design expressions for FRP-confined recycled tyre rubber concrete. Construct Build Mater. 2020;237:117633. https://doi.org/10.1061/j.conbuildmat.2019.117633
36. Ozbakkaloglu T, Akin E. Behavior of FRP-confined normal- and high-strength concrete under cyclic axial compression. J Compos Constr. 2014;16:451–63. https://doi.org/10.1061/(ASCE)CC.1943-5614.0000273
37. Dai J, Bai Y, Teng J. Behavior and modeling of concrete confined with FRP composites of large deformability. J Compos Constr. 2011;15:963–74. https://doi.org/10.1061/(ASCE)CC.1943-5614.0000230

38. Teng JG, Jiang T, Lam L, Luo YZ. Refinement of a design-oriented stress–strain model for FRP-confined concrete. J Compos Constr. 2009;13:269–78.
39. Lim JC, Ozbakkaloglu T. Confinement model for FRP-confined high-strength conrete. J Compos Constr. 2014;18(4):04013058. https://doi.org/10.1061/(ASCE)0733-9445(1988)114:8(1804)
40. Samaan M, Mirmiran A, Shahawy M. Model of concrete confined by fiber composites. J Struct Eng. 1994;124(9):1025–31.
41. Abbasnia R, Ziaadiny H. Behaviour of concrete prisms confined with FRP composites under axial cyclic compression. Eng Struct. 2010;32(648):655. https://doi.org/10.1016/j.endstruct.2009.11.011
42. Sima JF, Roca P, Molins C. Cyclic constitutive model for concrete. Eng Struct. 2008;30:695–706. https://doi.org/10.1016/j.engstruct.2007.05.005
43. Ziaadiny H, Abbasnia R. Unified cyclic stress-strain model for FRP-confined concrete circular, square and rectangular prisms. Struct Concr. 2016;17:220–35. https://doi.org/10.1002/suco.201500128
44. Chipperfield AJ, Fleming PJ. The MATLAB genetic algorithm toolbox. IEE Colloquium on Applied Control Techniques Using MATLAB, UK. London, UK: IET Digital Library; 1995.
45. Yu T, Zhang B, Teng TG. Unified cyclic stress–strain model for normal and high strength concrete confined with FRP. Eng Struct. 2015;102:189–201.
46. Palermo D, Vecchio FJ. Compression field modeling of reinforced concrete subjected to reverse loading: verification. ACI Struct J. 2004;101:155–64. https://doi.org/10.14359/12803
47. Freakley PK, Payne AR. Theory and practice of engineering with rubber. London: Applied Science Publishers; 1978.
48. Dong CX, Kwan AKH, Ho JCM. Effects of confining stiffness and rupture strain on performance of FRP confined concrete. Eng Struct. 2015;97:1–14. https://doi.org/10.1016/j.engstruct.2015.03.037
49. Dong CX, Kwan AKH, Ho JCM. A constitutive model for predicting the lateral strain of confined concrete. Eng Struct. 2015;91:155–66. https://doi.org/10.1016/j.engstruct.2015.02.014

AUTHOR BIOGRAPHIES

Samar Raffoul
School of Civil Engineering, University College Dublin, Dublin, Ireland.
Email: samar.raffoul@ucd.ie.

David Escolano Margarit
Department of Mechanical Engineering, Polytechnic University of Madrid, Calle José Gutiérrez Abascal, 2, Madrid 28006, Spain.
Email: d.escolano@upm.es.

Reyes Garcia
School of Engineering, The University of Warwick, Library Road, Coventry, CV4 7AL, UK.
Email: reyes.garcia@warwick.ac.uk.

Maurizio Guadagnini
Department of Civil and Structural Engineering, The University of Sheffield, Sir Frederick Mappin Building, Mappin Street, Sheffield, S1 3JD, UK
Email: m.guadagnini@sheffield.ac.uk.

Kypros Pilakoutas
Department of Civil and Structural Engineering, The University of Sheffield, Sir Frederick Mappin Building, Mappin Street, Sheffield, S1 3JD, UK.
Email: k.pilakoutas@sheffield.ac.uk.

How to cite this article: Raffoul S, Margarit DE, Garcia R, Guadagnini M, Pilakoutas K. A new cyclic model for FRP-confined rubberized concrete. Structural Concrete. 2022. https://doi.org/10.1002/suco.202200311